Electronic Supplementary Material (ESI) for Physical Chemistry Chemical Physics.

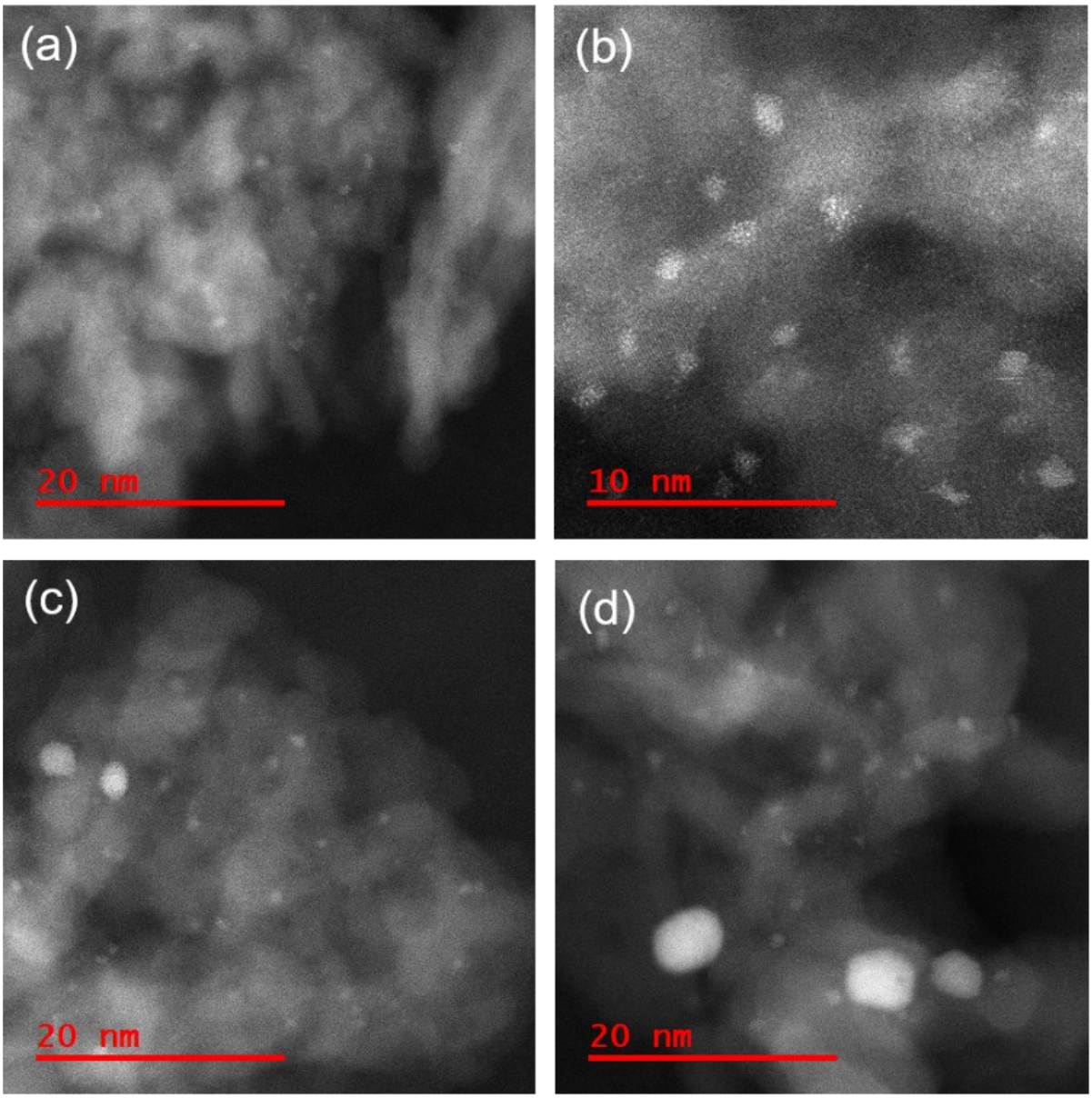

Figure S1. Typical Cs-STEM images of (a) 1.6 nm Pd/γ-Al_2O_3, (b) 2.6 nm Pd/γ-Al_2O_3, (c) 4.1 nm Pd/γ-Al_2O_3, and (d) 5.2 nm Pd/γ-Al_2O_3.

Table S1. Counted particle numbers of Pd/γ-Al_2O_3 in Figure S2.

Catalyst	Counted particle number
1.5 nm Pd/γ-Al_2O_3	245
1.6 nm Pd/γ-Al_2O_3	197
2.2 nm Pd/γ-Al_2O_3	370
2.6 nm Pd/γ-Al_2O_3	203
4.1 nm Pd/γ-Al_2O_3	418
5.2 nm Pd/γ-Al_2O_3	185
9.0 nm Pd/γ-Al_2O_3	147

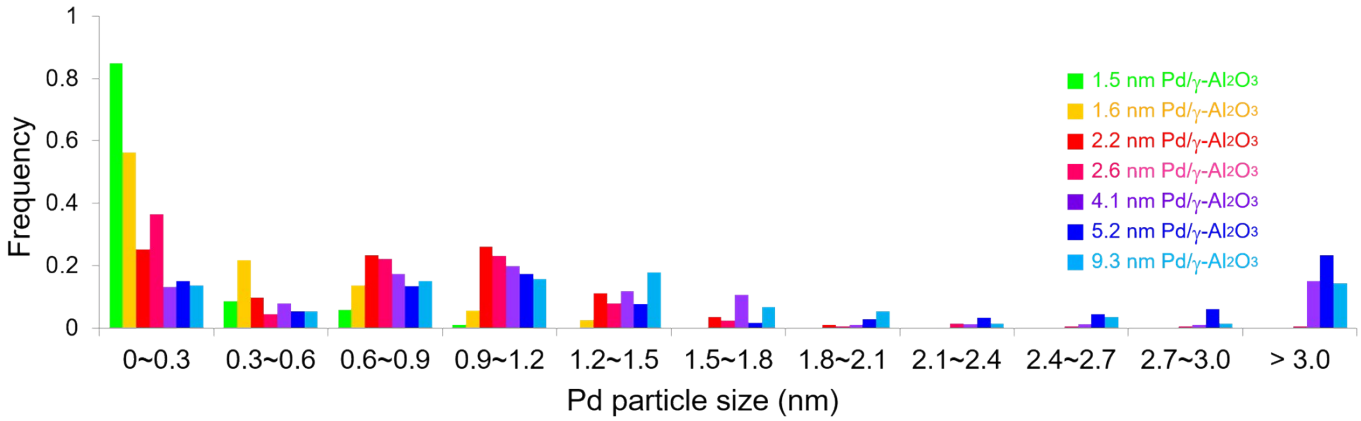

Figure S2. Size distributions for the number of Pd particles of various Pd/γ-Al_2O_3 catalysts.

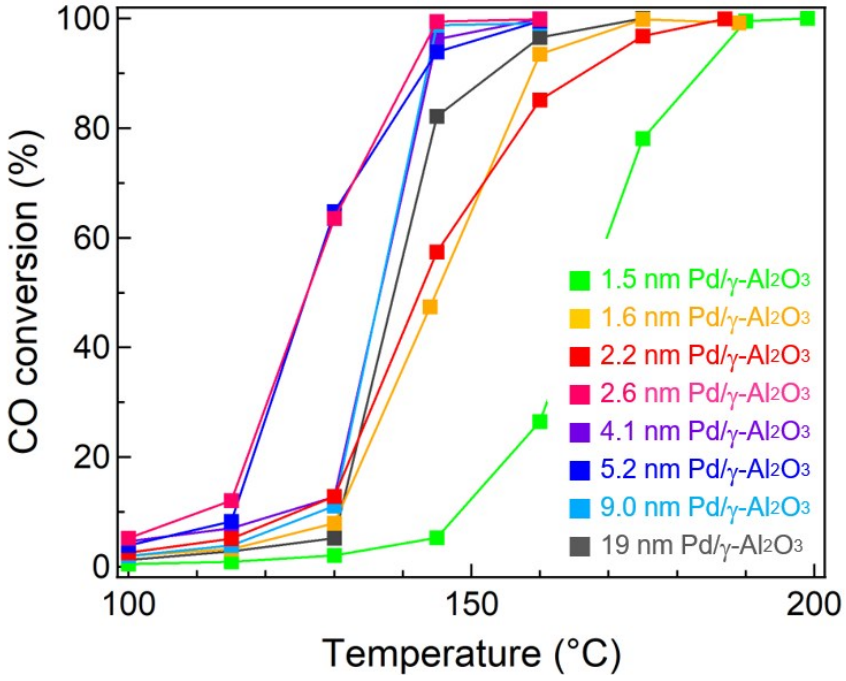

Figure S3. CO conversion over 10 mg of various Pd/γ-Al_2O_3 catalysts.

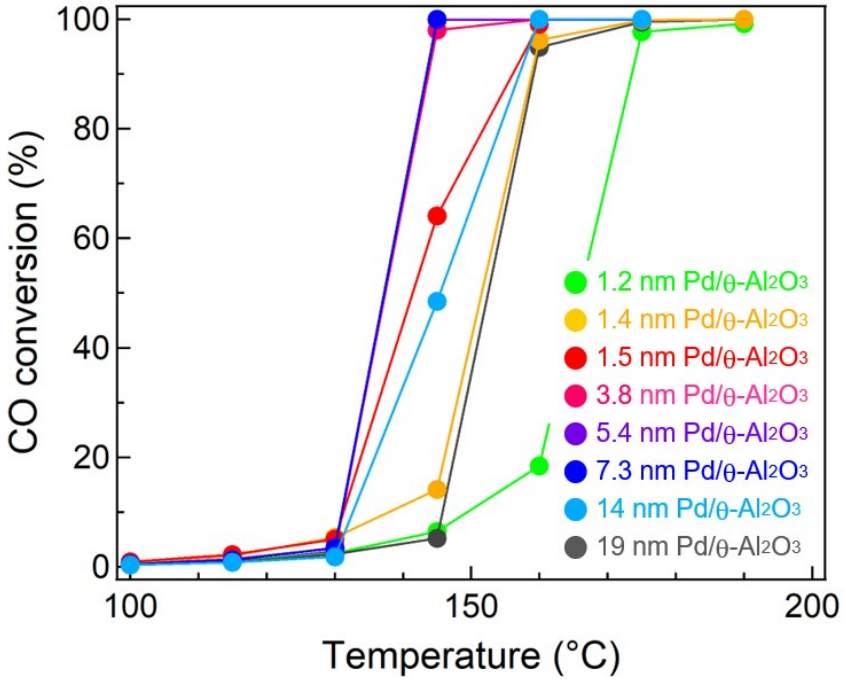

Figure S4. CO conversion over 10 mg of various Pd/θ-Al_2O_3 catalysts.

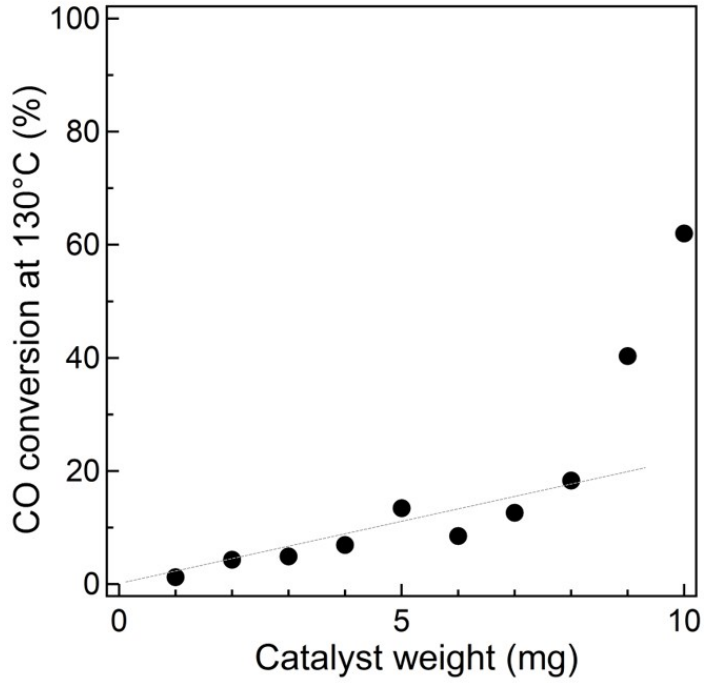

Figure S5. CO conversion at 130°C on various amounts of 2.2 nm Pd/γ-Al_2O_3. When the CO conversion on < 10 mg of the catalyst was evaluated, the catalyst powder was diluted with inert quartz powder to be 10 mg of powder in the tube reactor. A linear relationship between catalyst amount and CO conversion is seen on the figure in the range of < 20 % CO conversion. The data confirms that our kinetic analysis based on < 20 % CO conversion does not contain the problems due to thermal and gas diffusion effects.

Table S2. The list of data for TOF calculation

Catalyst	Catalyst weight[a] (mg)	Molar amount of surface Pd[b] ($\times 10^{-7}$ mol)	CO conversion (%)	CO oxidation rate[c] ($\times 10^{-8}$ mol·s^{-1})	TOF (s^{-1})
1.5 nm Pd/γ-Al_2O_3	10	0.66	1.7±0.2	0.51±0.06	0.076±0.010
1.6 nm Pd/γ-Al_2O_3	10	1.34	6.0±1.3	1.79±0.38	0.134±0.028
2.2 nm Pd/γ-Al_2O_3	10	2.53	15.1±2.7	4.49±0.80	0.177±0.032
2.6 nm Pd/γ-Al_2O_3	2	0.85	3.8±0.4	1.12±0.11	0.133±0.013
4.1 nm Pd/γ-Al_2O_3	2	1.03	4.4±2.6	1.30±0.79	0.079±0.010
5.2 nm Pd/γ-Al_2O_3	2	0.90	3.0±0.9	0.90±0.26	0.100±0.028
9.0 nm Pd/γ-Al_2O_3	10	2.35	8.5±1.7	2.52±0.52	0.107±0.022
19 nm Pd/γ-Al_2O_3	10	1.11	5.2	1.55	0.140
1.2 nm Pd/θ-Al_2O_3	10	0.91	2.5	0.74	0.081
1.4 nm Pd/θ-Al_2O_3	10	1.56	5.4	1.61	0.103
1.5 nm Pd/θ-Al_2O_3	10	3.42	5.0	1.49	0.044
3.8 nm Pd/θ-Al_2O_3	10	2.74	3.4	1.01	0.037
5.4 nm Pd/θ-Al_2O_3	2.5	0.99	0.9	0.28	0.028
7.3 nm Pd/θ-Al_2O_3	10	2.89	3.5	1.04	0.036
14 nm Pd/θ-Al_2O_3	10	1.47	1.8	0.54	0.037
19 nm Pd/θ-Al_2O_3	10	1.09	2.3	0.68	0.063

[a]Catalyst weight used to evaluate the TOF. [b]Molar amount of surface Pd (mol) was defined as (molar amount of Pd atom (mol)) / (Pd dispersion (%) / 100). [c]CO oxidation rate (mol·s^{-1})) was defined as (flow rate of CO molecule (mol·s^{-1}))×(CO conversion (%) / 100)

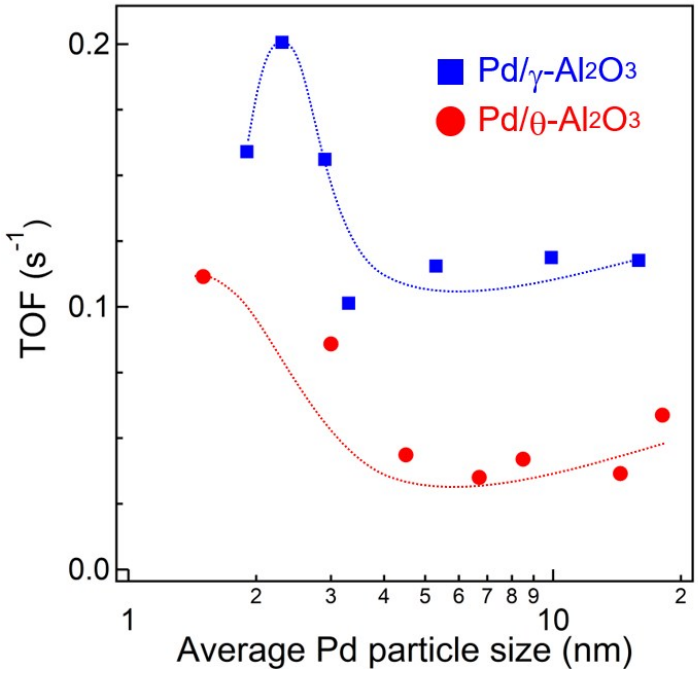

Figure S6. Dependence of TOF at 130°C on average Pd particle size estimated from H_2 pulse chemisorption. The 0.1wt% Pd/Al2O3 with high fraction of the isolated were excluded.

Table S3. The ratios of the IR band area of various CO species on Pd/Al_2O_3 catalysts.

Catalyst	Linear adsorbed CO on Pd^+ (2200-2100 cm^{-1})	Linear adsorbed CO on Pd^0 (2100-2000 cm^{-1})	Bridge adsorbed CO on Pd step (2000-1960 cm^{-1})	Bridge adsorbed CO on plane (1960-1700 cm^{-1})
1.5 nm Pd/γ-Al_2O_3	0.30	0.40	0.00	0.30
1.6 nm Pd/γ-Al_2O_3	0.09	0.44	0.00	0.47
2.2 nm Pd/γ-Al_2O_3	0.01	0.45	0.00	0.55
2.6 nm Pd/γ-Al_2O_3	0.05	0.33	0.00	0.63
4.1 nm Pd/γ-Al_2O_3	0.00	0.22	0.01	0.77
5.2 nm Pd/γ-Al_2O_3	0.00	0.23	0.02	0.76
9.0 nm Pd/γ-Al_2O_3	0.00	0.19	0.07	0.73
19 nm Pd/γ-Al_2O_3	0.00	0.28	0.09	0.63
1.2 nm Pd/θ-Al_2O_3	0.03	0.37	0.00	0.60
1.4 nm Pd/θ-Al_2O_3	0.01	0.45	0.00	0.53
1.5 nm Pd/θ-Al_2O_3	0.00	0.24	0.00	0.76
3.8 nm Pd/θ-Al_2O_3	0.00	0.09	0.18	0.73
5.4 nm Pd/θ-Al_2O_3	0.00	0.06	0.21	0.72
7.3 nm Pd/θ-Al_2O_3	0.00	0.05	0.20	0.76
14 nm Pd/θ-Al_2O_3	0.00	0.15	0.15	0.70
19 nm Pd/θ-Al_2O_3	0.00	0.22	0.15	0.63

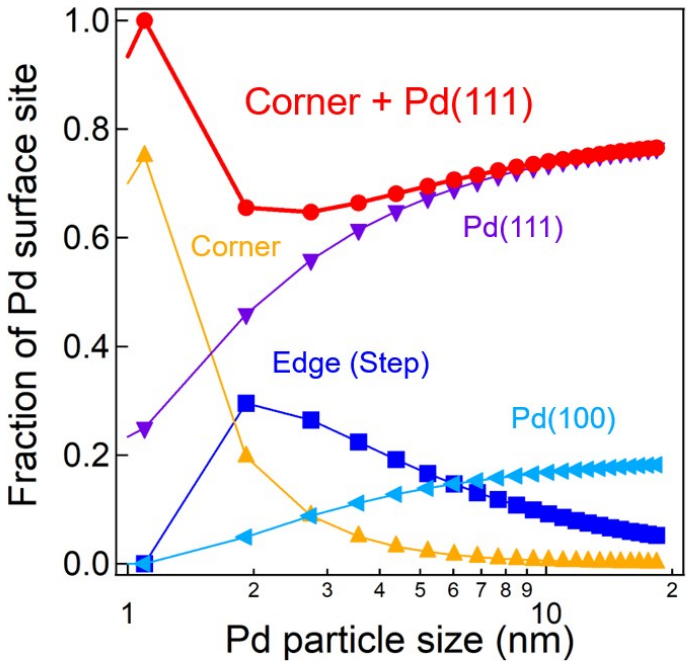

Figure S7. Particle size dependence of fraction of corner site and Pd(111) (●) and corner site (▲), Pd(111) (▼), Pd(100) (◀), edge site (or step) (■). We assumed a cubo-octahedron as a tentative model particle.

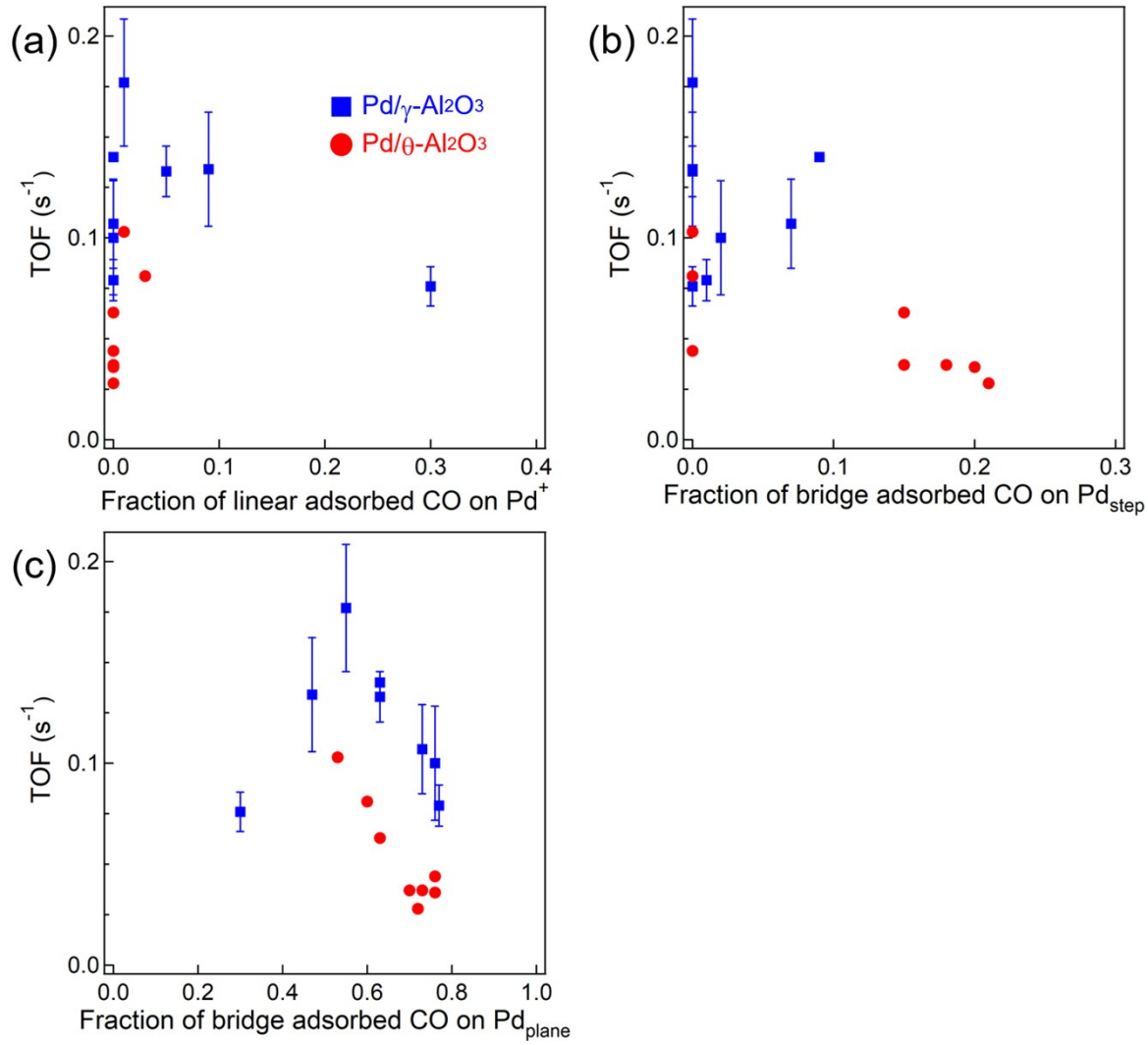

Figure S8. Plot of TOFs (at 130°C) against the fraction of (a) linear adsorbed CO on Pd^{+}, (b) bridge adsorbed CO on step site and (c) linear adsorbed CO on plane.

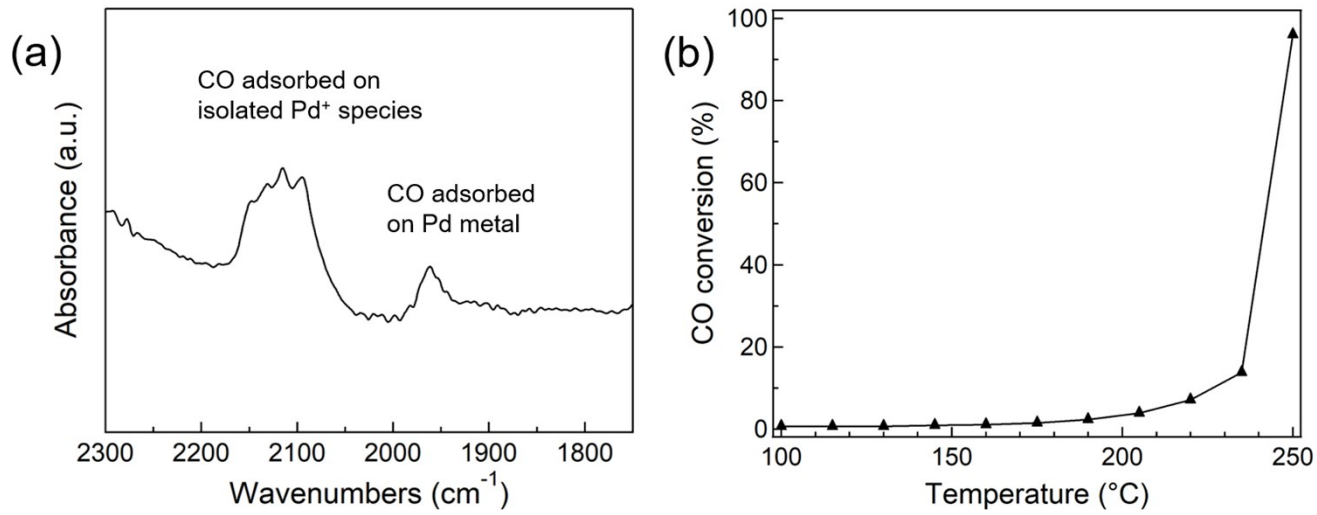

Figure S9. (a) IR spectra of adsorbed CO on Pd/ZSM-5. (b) The CO conversion of Pd/ZSM-5 as a function of temperature.

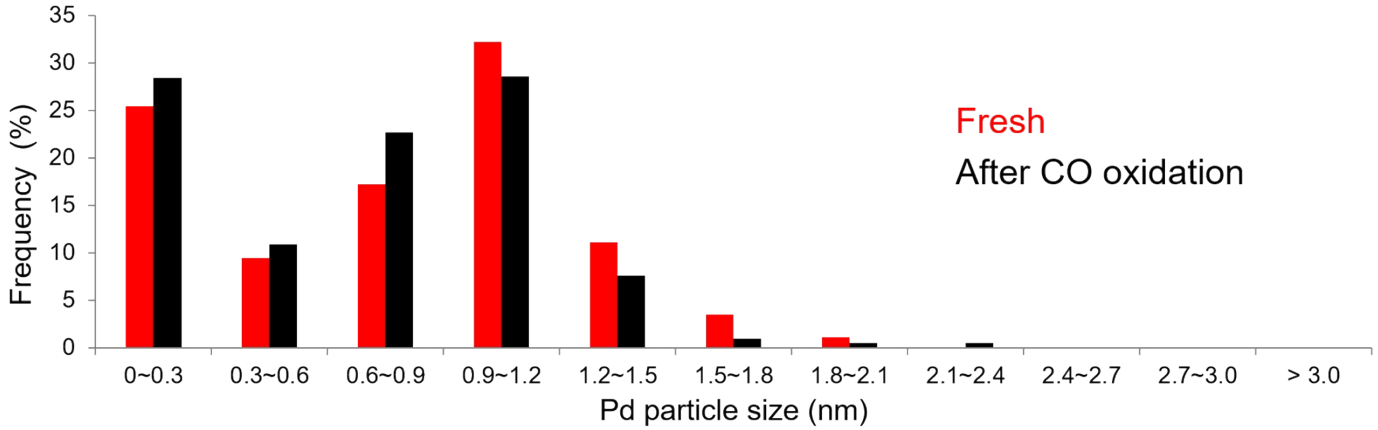

Figure S10. Size distributions for the number of Pd particles of 2.2 nm Pd/γ-Al_2O_3 catalyst after prereduction by H_2 (red) and CO oxidation reaction at 130°C (black).

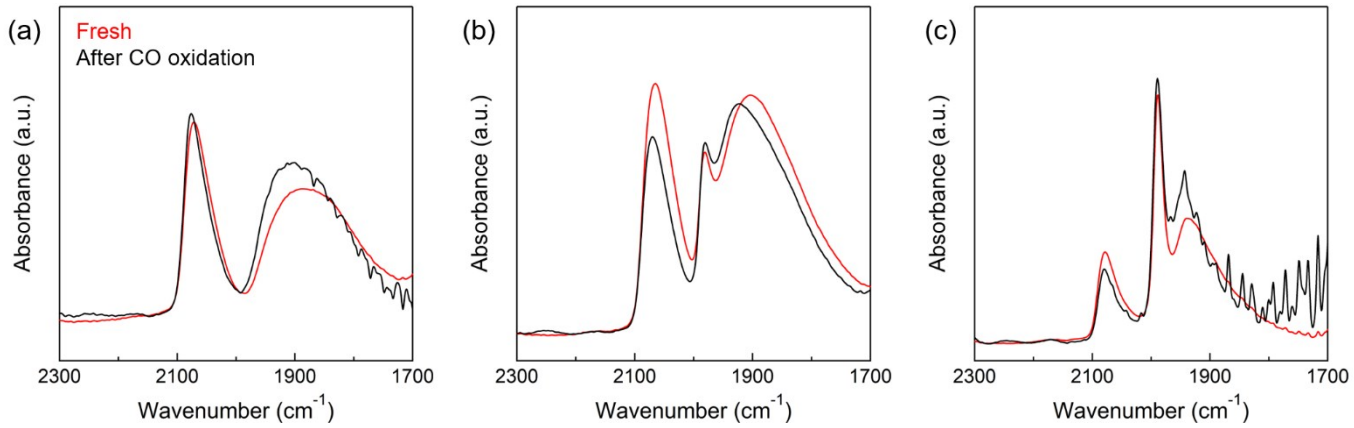

Figure S11. IR spectra of adsorbed CO on (a) 2.2 nm Pd/γ-Al_2O_3 and (b) 4.1 nm Pd/γ-Al_2O_3, (c) 5.4 nm Pd/θ-Al_2O_3 after prereduction by H_2 (red) and CO oxidation at 130°C (black).

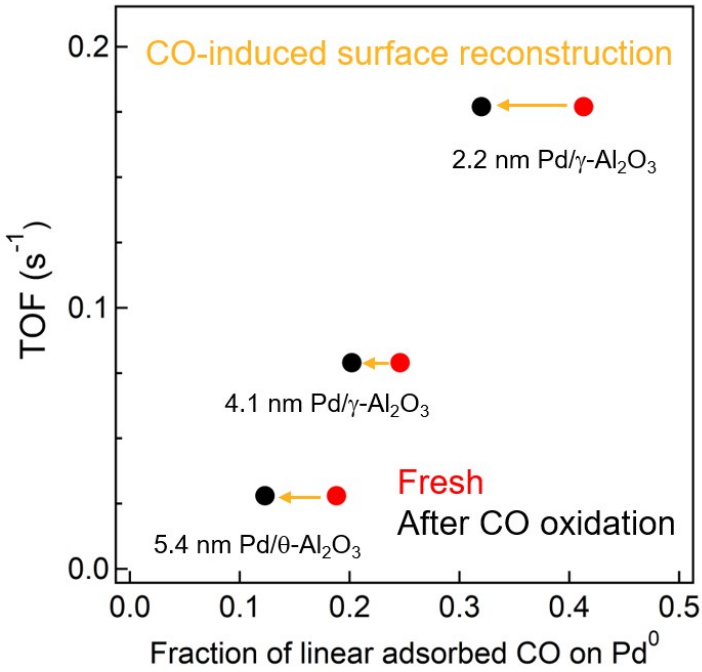

Figure S12. Plot of TOFs (at 130°C) against the fraction of linear adsorbed CO on Pd^0 for Pd/Al_2O_3 after prereduction by H_2 (red) and CO oxidation (black).

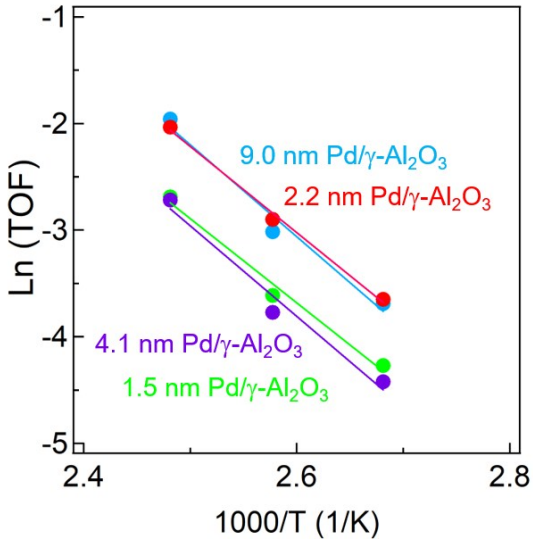

Figure S13. The dependence of TOFs on temperature for CO oxidation over Pd/γ-Al_2O_3.

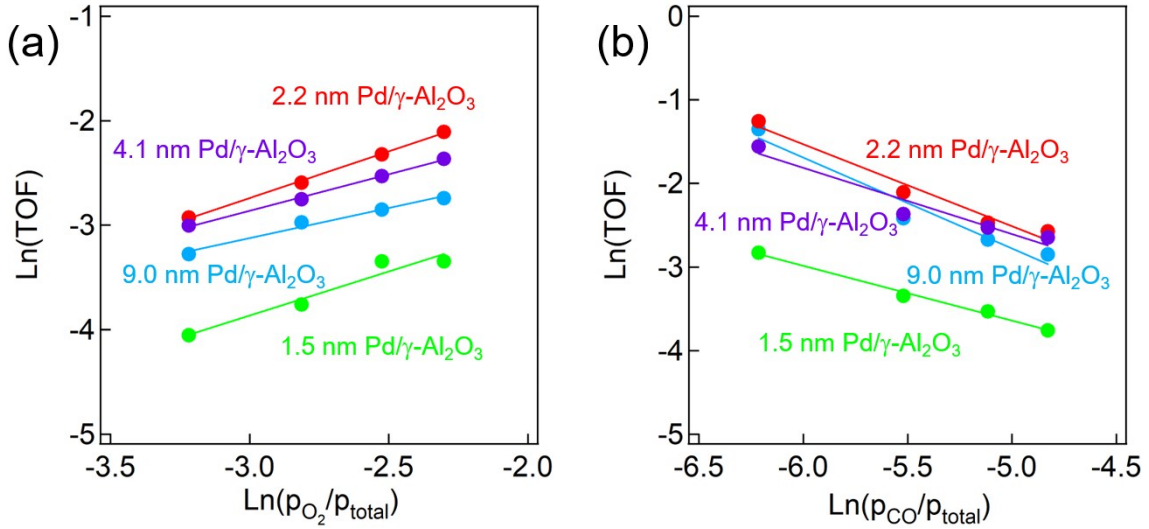

Figure S14. The dependence of TOFs on partial pressure of (a) O_2 and (b) CO for CO oxidation over Pd/γ-Al_2O_3.

Table S4. The apparent activation energy (E_a) and the reaction order for CO oxidation over Pd/γ-Al_2O_3.

Catalyst	E_a (kJ mol^{-1})	Reaction order of O_2	Reaction order of CO
1.5 nm Pd/γ-Al_2O_3	66±8	0.84±0.15	-0.66±0.04
2.2 nm Pd/γ-Al_2O_3	66±7	0.89±0.02	-0.98±0.12
4.1 nm Pd/γ-Al_2O_3	71±11	0.69±0.03	-0.79±0.15
9.0 nm Pd/γ-Al_2O_3	72±11	0.58±0.06	-1.08±0.18

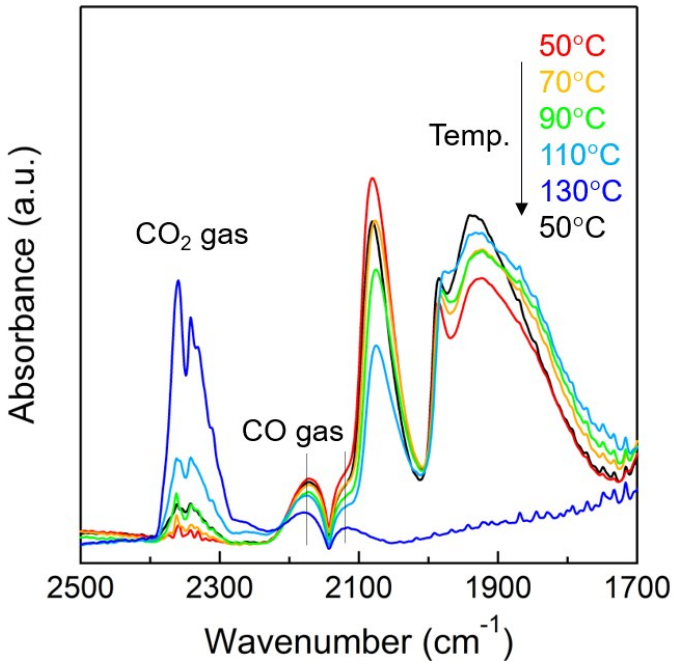

Figure S15. IR spectra of adsorbed CO on 4.1 nm Pd/γ-Al_2O_3 measured under a flow of gaseous mixtures (0.4% CO, 10% O_2, Ar balance, 100 mL/min) at various temperatures.